



Article scientifique

Article

2020

Accepted version

Open Access

This is an author manuscript post-peer-reviewing (accepted version) of the original publication. The layout of the published version may differ .

Measuring slow heteroaggregation rates in the presence of fast homoaggregation

Cao, Tianchi; Trefalt, Gregor; Borkovec, Michal

How to cite

CAO, Tianchi, TREFALT, Gregor, BORKOVEC, Michal. Measuring slow heteroaggregation rates in the presence of fast homoaggregation. In: Journal of Colloid and Interface Science, 2020, vol. 566, p. 143–152. doi: 10.1016/j.jcis.2020.01.075

This publication URL: <https://archive-ouverte.unige.ch/unige:134082>

Publication DOI: [10.1016/j.jcis.2020.01.075](https://doi.org/10.1016/j.jcis.2020.01.075)

Revised, January 17, 2020

Published in J. Colloid Interf. Sci. 566, 2020, 143-152

DOI : 10.1016/j.jcis.2020.01.075.

Measuring slow heteroaggregation rates in the presence of fast homoaggregation

Tianchi Cao, Gregor Trefalt and Michal Borkovec*

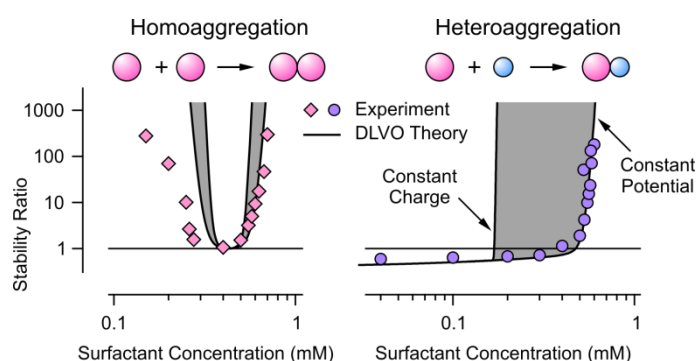
Department of Inorganic and Analytical Chemistry, University of Geneva, Sciences II,
30 Quai Ernest-Ansermet, 1205 Geneva, Switzerland

*Corresponding author, Email: michal.borkovec@unige.ch

Abstract

Homoaggregation and heteroaggregation involving amidine and sulfate latex particles in the presence of the anionic surfactant octyl sulfate (OS) is studied by light scattering. This surfactant causes a charge reversal of the amidine particles. This reversal induces a rapid homoaggregation near the charge reversal point. In the presence of the same surfactant, the sulfate particles remain negatively charged and stable. The heteroaggregation process is probed in mixed suspensions of amidine and sulfate latex particles with multi-angle time-resolved dynamic light scattering. This technique allows differentiating between the contributions of homoaggregation and heteroaggregation, and permits to measure the heteroaggregation rate. By optimally choosing the sizes of the particles, one can optimize the contrast and extract heteroaggregation stability ratio over a wide range. The heteroaggregation rate is fast at low OS concentrations, where the two particles are oppositely charged. This rate slows down at higher OS concentrations due to double layer repulsion between the negatively charged particles. However, the onset of this slow heteroaggregation occurs at lower OS concentrations than for homoaggregation. The reason for this shift is that the double layer repulsion between two OS-decorated amidine particles is weaker than between one sulfate particle and one OS-decorated amidine particle. These measurements compare favorably with calculations with the theory by Derjaguin, Landau, Verwey, and Overbeek (DLVO). These calculations suggest that constant potential boundary conditions are more appropriate than the ones of constant charge. In the system studied, the present light scattering technique permits to extract heteroaggregation stability ratios over almost three orders of magnitude. This study is the first of its kind, where such a large range is being probed.

Graphical Abstract



Keywords

Heterocoagulation, latex particles, colloidal stability, electrophoresis, DLVO theory

Introduction

Numerous studies focus on colloidal aggregation, but researchers normally investigate aggregation of the same kind particles, referred to as homoaggregation [1-8]. Such investigations are surely of great importance, as many applications involve precisely such systems, for example, in ceramic processing, formulation of drugs, or fabrication of paints [9-11]. However, at least as many applications concern aggregation in systems involving two or more types of particles, referred to as heteroaggregation. Notable examples are food processing, papermaking, water treatment, or groundwater remediation [12-15]. Aggregation processes in such mixed particle systems are much less understood.

The simplest example of such a mixed system consists of a binary suspension involving two types of particles [16-25]. The early stages of particle aggregation are governed by the formation of particle dimers, while larger aggregates form at later stages of aggregation. In the early stages of aggregation in a binary suspension, three types of dimers may form, namely two types of symmetric homoaggregates, and one type of heteroaggregate.

While many experimental techniques are available to probe homoaggregation processes reliably, to study heteroaggregation processes remains challenging. The main obstacle is to properly distinguish the formation of homoaggregates and heteroaggregates. One approach is single particle counting [26-28]. Thereby, one forces the aggregating suspension through a narrow capillary, and then one is able to probe one particle aggregate after another, typically through conductivity or light scattering. While this technique normally achieves an excellent resolution, and is often able to distinguish various types of aggregates, it is very slow and may disrupt the aggregates through the high shear rates present.

The other approach is to use time-resolved light scattering techniques [18-25]. While such techniques are well established to probe homoaggregation processes in situ, they have not been widely used to investigate heteroaggregation processes. One possible approach is to measure an apparent aggregation rate, and to vary the fractions of the two types of particles [18-22]. The presence of heteroaggregation leads to a characteristic dependence of the apparent aggregation rate on this fraction, from which the heteroaggregation rate can be extracted. However, this approach is very laborious, as for each condition several different suspensions must be prepared and analyzed.

Here we take another approach, and exploit the different angular dependencies of the scattering profiles of the different aggregates [23-25]. In particular, when the size of the particles involved is chosen appropriately, the different dimers can be distinguished through their characteristic angular variation of the scattering signal. Such studies were already carried out in the past, and it was indeed possible to extract heteroaggregation rates over wide range of conditions [24,25]. However, the drawback of all these approaches was that the contrast between the different aggregates was poor, and

therefore heteroaggregation rates were not accessible over a very wide range, typically over one order of magnitude or less.

In the present study we will demonstrate that by appropriate choice the particles involved, the contrast between the different aggregates can be substantially enhanced. This approach enables us to measure heteroaggregation rates over a much wider range, and as we shall demonstrate, almost three orders of magnitude can be covered. These measurements will be further confronted with calculations based on the theory established by Derjaguin, Landau, Verwey, and Overbeek (DLVO) [1,2].

Methods

Extracting aggregation rates from light scattering. Early stages of aggregation are governed by the formation of particle dimers from particle monomers. In a binary mixture of monodisperse and spherical colloidal particles of type A and B, three possible particle dimers may form. There are two types of homoaggregates AA and BB, and one heteroaggegate AB. This process is conveniently probed by multi-angle time-resolved dynamic light scattering, whereby one measures the apparent dynamic rate

$$\Delta(\theta) = \frac{1}{R(\theta,0)} \cdot \left. \frac{dR(\theta,t)}{dt} \right|_{t \rightarrow 0} \quad (1)$$

where $R(\theta,t)$ is the apparent hydrodynamic radius, which depends on the experimental time t and the scattering angle θ . The three aggregation processes contribute to this quantity in an additive fashion, namely [23-25]

$$\Delta(\theta) = k_{AA}H_{AA}(\theta) + 2k_{AB}H_{AB}(\theta) + k_{BB}H_{BB}(\theta) \quad (2)$$

where k_{ij} are the aggregation rate coefficients for the formation of respective particle dimer of type ij , and $H_{ij}(\theta)$ are characteristic functions that are dependent of the scattering angle. The subscripts i and j refer to the particles A and B. This function can be represented as a difference of two other functions [24,25]

$$H_{ij}(\theta) = F_{ij}(\theta) - G_{ij}(\theta) \quad (3)$$

where the first function is given by

$$F_{ij}(\theta) = \frac{N_0 x_i x_j}{2} \cdot \frac{I_{ij}(\theta) - I_i(\theta) - I_j(\theta)}{x_A I_A(\theta) + x_B I_B(\theta)} \quad (4)$$

where $I_{ij}(\theta)$ is the scattering intensity of the particle dimer of type ij and $I_i(\theta)$ the corresponding quantity for the particle monomer of type i . The quantities x_i are the number fractions of the particles of type i and N_0 is the total particle number concentration of both types of particles. The second function is given by

$$G_{ij}(\theta) = \frac{N_0 x_i x_j}{2} \cdot \frac{I_{ij}(\theta) / R_{ij} - I_i(\theta) / R_i - I_j(\theta) / R_j}{x_A I_A(\theta) / R_A + x_B I_B(\theta) / R_B} \quad (5)$$

where is the R_{ij} hydrodynamic radius of the particle dimer, and R_i the hydrodynamic radius of the particle monomer of type i . Note further that $x_A + x_B = 1$. These characteristic functions are given here without derivation and we refer to the literature for further details [24,25].

For spherical particles, the scattering intensities and hydrodynamic radii can be calculated. The scattering intensities of the particle monomers can be evaluated with Mie theory and the ones of the particle dimers with T-matrix theory [29,30]. For monodisperse particles, the hydrodynamic monomer radius R_i is further identical to the particle radius. The hydrodynamic radius of the dimers are obtained with the empirical formula [25,31]

$$\alpha_{ij} = \frac{2R_{ij}}{R_i + R_j} = 1.392 + 0.608 \cdot \left(\frac{R_i - R_j}{R_i + R_j} \right)^2 \quad (6)$$

This formula accurately represents the exact results obtained from the analysis of the diffusion coefficients at low Reynolds numbers of pairs of unequal spheres [32]. To align with previous studies, we report the aggregation rate coefficients in terms of the stability ratios defined as

$$W_{ij} = \frac{k_{ij}^{(\text{fast})}}{k_{ij}} \quad (7)$$

where k_{ij} and $k_{ij}^{(\text{fast})}$ are the experimental and fast aggregation rate coefficients, respectively.

Materials. Samples of amidine latex (AL) and sulfate latex (SL) of low polydispersities were purchased from Invitrogen corporation. The same batches of particles were extensively characterized by static and dynamic light scattering as described in a previous study [33]. Table 1 summarizes the respective particle radius and polydispersity, which is expressed as the coefficient of variation (CV). Before use, the particle suspensions were dialyzed for about one week in Milli-Q water (Millipore) until the conductivity of the surrounding solution dropped below 80 $\mu\text{S/m}$. For the dialysis, polyvinylidene fluoride and cellulose ester membranes were used for the AL and SL particles,

respectively. Analytical grade sodium n-octyl sulfate (OS, Alfa Aesar) and NaCl (Sigma-Aldrich) were dissolved with Milli-Q water (Millipore) and adjusted to pH 4.0 with HCl.

Light scattering experiments. Electrophoretic light scattering was carried out with the respective particle suspensions with Zetasite Nano ZS (Malvern Instruments). Suspensions were prepared by adding a small aliquot of the dialyzed latex suspension to the solution containing the appropriate amount of OS and NaCl. The particle concentrations were 0.50 mg/L ($3.4 \times 10^{14} \text{ m}^{-3}$) for the AL particles and 0.23 mg/L ($3.3 \times 10^{14} \text{ m}^{-3}$) for SL. The electrophoretic mobility was extracted from the experiments and converted to the electrokinetic potential (ζ -potential) with the theory of O'Brien and White [34].

A multi-angle light scattering goniometer (ALV, CGS-8F) was used to measure the aggregation rates. The goniometer uses 8 fiber-optic detector and a solid-state laser operating at a wavelength of 532 nm and we use an angular resolution of 4.25° . Borosilicate cuvetts were used to carry out the experiments, which were first cleaned with hot piranha solution, which was prepared by mixing concentrated H_2SO_4 and 30% H_2O_2 in a volume ratio 3:1. Then they were washed in plenty of Milli-Q water and dried at 60°C in a dust-free oven. The aggregation process was initiated by injecting the respective particle suspensions into the solutions containing OS and NaCl, and subsequent rapid mixing. For each time point, the light scattering signals were accumulated during 20 s, and the hydrodynamic radii were extracted from the second cumulant fit of the correlation function by means of the Stokes-Einstein relation. The aggregation was typically monitored over 30 min. For each scattering angle θ , the dynamic rate was extracted by fitting the time dependence of the apparent hydrodynamic radius $R(\theta, t)$ with a straight line, and dividing its slope by the intercept at the beginning of the experiment. All experiments were carried out in the early stages of the aggregation process. This condition was ensured that the hydrodynamic radius did not increase by more than 30% during the overall measurement time. Heteroaggregation experiments were carried out in mixed suspensions of AL and SL particles at particle concentrations of 0.5 mg/L and 0.23 mg/L, respectively. These concentrations correspond to a total particle concentration of $6.6 \times 10^{13} \text{ m}^{-3}$ and an AL particle number fraction of 0.51. Homoaggregation experiments were carried out in suspensions of one particle type, whereby the particle concentrations used were 0.5 mg/L ($3.4 \times 10^{13} \text{ m}^{-3}$) for AL and 0.23 mg/L ($3.3 \times 10^{13} \text{ m}^{-3}$) for SL. The respective stability ratios were determined with time-resolved dynamic light scattering at a scattering angle of 90° . Similar measurements of this type were described in detail earlier [4,33].

Calculation of aggregation rates with DLVO theory. Aggregation rate coefficients are obtained from the steady-state solution of the diffusion equation for a particle pair i and j interacting by means of a conservative interaction potential energy $V_{ij}(h)$, where h is the closest separation distance. The aggregation rate coefficient can be expressed as [1,24]

$$k_{ij} = \frac{4}{3\beta\eta\sigma_{ij}} \left[\int_0^{\infty} \frac{B_{ij}(h)e^{\beta V_{ij}(h)}}{(R_i + R_j + h)^2} dh \right]^{-1} \quad (8)$$

where η is the shear viscosity, $\beta = 1/(k_B T)$ is the inverse thermal energy, with k_B being the Boltzmann constant and T the absolute temperature, and σ_{ij} is defined by $2\sigma_{ij}^{-1} = R_i^{-1} + R_j^{-1}$. The hydrodynamic resistance function is approximated as

$$B_{ij}(h) = \frac{6h^2 + 13\sigma_{ij}h + 2\sigma_{ij}^2}{6h^2 + 4\sigma_{ij}h} \quad (9)$$

The temperature is set at 25°C and accordingly $\eta = 8.9 \times 10^{-4}$ Pas. The particle interaction energy is obtained within the Derjaguin approximation as [1,24]

$$V_{ij}(h) = \pi\sigma_{ij} \int_h^{\infty} \int_{h'}^{\infty} \Pi(h'') dh'' dh' \quad (10)$$

where $\Pi(h)$ is the pressure between two planar walls, which have the same surface and bulk properties as the particles involved. DLVO theory suggests that the pressure can be decomposed as [1,24]

$$\Pi(h) = \Pi_{\text{vdw}}(h) + \Pi_{\text{dl}}(h) \quad (11)$$

where $\Pi_{\text{vdw}}(h)$ is the contribution from van der Waals and $\Pi_{\text{dl}}(h)$ from double-layer interactions. The former contribution is calculated within the non-retarded approximation [1]

$$\Pi_{\text{vdw}}(h) = -\frac{H}{6\pi} \cdot \frac{1}{h^3} \quad (12)$$

where H is the Hamaker constant. Double layer forces are obtained from the numerical solution of the full Poisson-Boltzmann (PB) equation [1,35]. This equation relates the electrostatic potential profile $\psi(x)$, which depends on the position x in between the plates situated at $x = \pm h/2$. In the case of a monovalent electrolyte of concentration c , the PB equation reads [1]

$$\frac{d^2\psi}{dx^2} = \frac{\kappa^2}{\beta q} \sinh(\beta q \psi) \quad (13)$$

where q is the elementary charge and we use the abbreviation

$$\kappa^2 = \frac{2\beta q^2 c}{\varepsilon_0 \varepsilon} \quad (14)$$

where ε_0 is the permittivity of vacuum, and ε the dielectric constant of water, where we use $\varepsilon = 80$. Thereby, κ^{-1} corresponds to the Debye length. Equation (13) is solved subject to the boundary conditions

$$\pm \varepsilon_0 \varepsilon \frac{d\psi}{dx} \Big|_{x=\pm h/2} = \sigma_{\pm} - C_{\text{in}}^{(\pm)} [\psi(\pm h/2) - \psi_{\pm}] \quad (15)$$

where σ_{\pm} , ψ_{\pm} , and $C_{\text{in}}^{(\pm)}$ are the surface charge density, diffuse layer potential, and the inner capacitance of the respective isolated surfaces. We express the regulation properties of each surface in terms of the regulation parameter

$$p_{\pm} = \frac{C_{\text{dl}}^{(\pm)}}{C_{\text{dl}}^{(\pm)} + C_{\text{in}}^{(\pm)}} \quad (16)$$

where $C_{\text{dl}}^{(\pm)}$ is the diffuse layer capacitance. For the classical boundary conditions of constant potential (CP) and constant charge (CC), the regulation parameter is $p_{\pm} = 0$ and 1, respectively. The solution of the PB equation is obtained numerically for given separation h with a deferred correction Newton iteration technique [36]. Once the electrostatic potential profile $\psi(x)$ is known, the pressure generated by the double layer can be calculated from

$$\Pi_{\text{dl}} = 2k_{\text{B}}T[\cosh(\beta q\psi) - 1] - \frac{\varepsilon_0 \varepsilon}{2} \left(\frac{d\psi}{dx} \right)^2 \quad (17)$$

The stability ratios are obtained from eq. (7) where $k_{ij}^{(\text{fast})}$ is obtained by considering van der Waals forces only.

Results and Discussion

Heteroaggregation rate coefficients were measured with time-resolved multi-angle dynamic light scattering in the past [23-25]. In all these studies, however, the rates of homoaggregation and heteroaggregation were quite comparable. As a consequence, range of the measured heteroaggregation stability ratios remained small, typically one order of magnitude, or less [25]. In the present study, we show how this range can be substantially expanded by choosing an appropriate particle pair, and we will report reliable measurements of heteroaggregation stability ratios spanning a much wider range. We will first demonstrate how T-matrix calculations can be used to choose optimal contrast for a given particle pair. Subsequently, an appropriate particle pair of monodisperse amidine latex (AL) and sulfate latex (SL) particles is chosen, and respective heteroaggregation rate measurements are carried

out. These measurements are complemented with the respective homoaggregation and electrophoresis measurements. As we shall demonstrate, by optimizing the contrast between the two particles, heteroaggregation stability ratios can be measured over almost three orders of magnitude.

Choosing an optimal particle pair. Difficulties with heteroaggregation rate measurements with multi-angle time-resolved light scattering often occur, when one type of particles is highly charged, but the other one weakly. Under these conditions, there is no homoaggregation between the highly charged particles. However, one should be able to distinguish heteroaggregation from the homoaggregation between the weakly charged particles. This distinction can be challenging, since under these conditions homoaggregation is typically fast, while heteroaggregation can be slow, and thus the signal is dominated by the homoaggregation processes. This dominance of the signal from homoaggregation is the main reason, why a recent study on heteroaggregation did not report any heteroaggregation stability ratios above 10 [25].

This problem can be largely circumvented, however, by choosing the size of the two types of particles appropriately. In order to have a sensible contribution from both types of particles, their sizes must be comparable. In this case, they should also be mixed in comparable quantities. To analyze the situation further, detailed calculations with the T-matrix theory must be carried out. Figure 1 shows the expected apparent dynamic rates versus the scattering angle, whereby the contributions of the different dimers are also indicated. The subfigures reflect different particle radii. Thereby, the columns show the same ratios of the particle radii, while the rows different overall radii. The calculations are carried out for monodisperse particles and the present experimental setup. All three aggregation rate coefficients are chosen to be the same, and the number fraction of each particle is chosen 0.5. The larger particles are denoted with the symbol A, while the smaller one with B.

Let us first focus on the effect of the overall particle size as illustrated in the different rows of Fig. 1. Particles with radii below 100 nm show only modest angular variations, but for radii over 200 nm these variations become very pronounced, and the response tends to oscillate. The resolution of these oscillations would require a very high angular resolution, which is difficult to achieve. Therefore, intermediate particle radii around 150 nm are most suitable. Let us now fix the radius of the larger particle A to this value, and investigate the effect of variations of the radius of the smaller particle B. This variation is shown in the middle row of Fig. 1. When the size disparity is too small, homoaggregates AA and BB contribute in the entire accessible angular range substantially. For intermediate size disparities, one observes that near a scattering angle of 110° the response of the heteroaggregates AB shows a maximum. A similar maximum occurs for the homoaggregate BB, but the homoaggregate AA shows a minimum. When the aggregation process can be tuned such that no homoaggregates BB are forming, one would expect to be able to distinguish heteroaggregates AB

from the homoaggregates AA easily. When the size disparity becomes too large, the contribution from homoaggregates AA becomes more important, especially at smaller angles. For this reason, a pair of particles A and B with radii around 150 nm and 120 nm should be suitable to obtain a good contrast. At the same time, the formation of homoaggregates BB involving the smaller particles must be suppressed.

The other important variable is mixing ratio of the two particle types, which we express as the number fraction of the larger particles x_A . The influence of this fraction for the two particle radii 150 nm and 120 nm is shown in Fig. 2. This fraction is indicated in each subfigure, and it increases from left to right and from the top to bottom. Clearly, when this fraction is either 0 or 1, one only observes the contribution of the respective homoaggregates. As the fraction is increased, the contribution from AA homoaggregates increases, while the one from BB homoaggregates decreases. The AB heteroaggregates only contribute for intermediate fractions. One observes that the minimum for the AA homoaggregates occurring near a scattering angle of 110° is preserved for intermediate particle fractions between 0.4 and 0.6. Thus any fraction within this range is suitable.

Guided by these calculations we have chosen to study suspensions of monodisperse amidine latex (AL) with a radius near 150 nm and sulfate latex (SL) particles with a radius near 120 nm, see Table 1. The scattering calculations were corrected for polydispersities, and the respective radii and coefficients of variation (CV) determined by static light scattering were used throughout. Note that same particles were also used in a previous study [33]. In the present experiments, the number fraction of the AL particles was chosen to be 0.51. In particular, heteroaggregation will be studied in the presence of an anionic surfactant, which strongly adsorbs to the positively charged AL particles, and thereby induces their charge neutralization. In the presence of the same surfactant, the SL particles remain highly negatively charged. As a consequence, the formation of the SL-SL homoaggregates is suppressed, while only the homoaggregates AL-AL together with the heteroaggregates AL-SL will form. Under these conditions, the heteroaggregation rates can be measured over a wide range.

Measurements in sodium chloride solutions. Let us first demonstrate that in the presence of a simple monovalent salt NaCl, the present system shows analogous trends as reported earlier [24,25]. Figure 3 shows the dependence on the salt concentration of the electrokinetic potentials, which were extracted from electrophoretic mobility measurements. One observes that the AL particles are positively charged, while the SL particles negatively. The sign of the potential can be easily understood by considering the chemical nature of the surface groups, since the amidine groups are positively charged, and the sulfate groups negatively. The magnitude of the potential of the AL particles is higher, suggesting that the magnitude of the charge is higher for AL particles than for SL. Moreover, the potential of AL particles goes through a maximum. This maximum might be caused by progressive protonation of dissociable

surface groups with decreasing salt concentration, which causes a reduction of the surface charge density at lower salt levels, and thus induces a lower surface potential.

We have first studied the homoaggregation process in suspensions of AL or SL particles suspended in NaCl solutions. Similar investigations were already described in a previous study [33], but here these results will be compared with T-matrix calculations.

The stability ratios for homoaggregation are shown in Fig. 4a,b. One observes the typical behavior reported for charged latex particles in earlier studies [24]. At high salt concentrations, the aggregation rate is fast, and independent of the salt concentration. By definition, the stability ratio is unity in this regime. With decreasing salt concentration, the stability ratio increases steeply and the aggregation becomes slow. At 10 mM and below, the suspensions are perfectly stable. The transition between slow and fast aggregation is referred to as the critical coagulation concentration (CCC). For both systems, the CCC is around a NaCl concentration of 0.15 M [33].

Let us now focus on the analysis of the absolute homoaggregation rates under fast conditions. These conditions were realized in 0.8 M NaCl. The rate coefficients were extracted with T-matrix theory. These results are summarized in Fig. 5a,b. These figures show the apparent dynamic rates for the homoaggregation process in suspensions containing AL or SL particles, respectively. The T-matrix theory describes the measured angle dependence very well. Note that the fit involves only one adjustable parameter, namely the respective aggregation rate coefficient. Adjusting this coefficient only changes the overall magnitude of the apparent rate, but not its characteristic angular dependence. We also remark that for the AL and SL particles the angular dependence of the apparent dynamic rates is very different.

The fitted homoaggregation rate coefficients are given in Table 2. One observes that these coefficients are very similar. In particular, these numbers agree with the fast aggregation rate coefficients for the same particles measured in 0.6 M NaCl solutions are within experimental error [33]. However, the latter number were determined without making any assumptions about the actual optical response of the particles, and it is comforting to see that T-matrix calculations yield the same results.

To study the heteroaggregation process, a mixed suspension of AL and SL particles was investigated in 10 mM NaCl solution. Figure 4a,b shows that under these conditions the stability ratios for homoaggregation exceed 100 for both types of particles, and therefore this process can be safely neglected. Since the particles are oppositely charged, however, under these conditions only heteroaggregation occurs. Figure 5c confirms that this is indeed the case. This figure compares the measured apparent dynamic rate with the T-matrix theory calculation for the heteroaggregates. The very good agreement indicates that only these aggregates form. One can again adjust the

heteroaggregation rate coefficient, and one finds that this coefficient is $(4.6 \pm 0.2) \times 10^{-18} \text{ m}^3/\text{s}$. This experiment further confirms that the T-matrix theory describes the optical response of the heteroaggregates very well.

To determine the heteroaggregation rate coefficient in the fast aggregation conditions, a similar experiment was carried out in 0.8 M NaCl solution. The result is shown in Fig. 5d. Now both homoaggregation processes occur together with the heteroaggregation processes. However, the homoaggregation rate coefficients are known under these conditions, and thus the only unknown is the heteroaggregation rate coefficient. Adjusting this parameter one obtains an excellent fit of the experimental data, and the respective rate coefficient can be extracted. This number is reported in Table 2, and is very comparable to the homoaggregation rate coefficients.

With this number at hand, one can also calculate the stability ratios for heteroaggregation. The available values are reported in Fig. 4c. Heteroaggregation remains fast, but the stability ratio decreases slightly with decreasing salt level. This decrease is due to the salt dependence of the double layer attraction between two oppositely charged surfaces. This attraction strengthens with decreasing ionic strength, which lead to a decrease in the stability ratio with decreasing salt concentration. Very similar trends in the heteroaggregation between oppositely charged particles were already reported earlier [23-25].

Measurements in sodium octyl sulfate (OS) solutions. Let us now address the aggregation behavior of these particles in solutions containing the short-chain anionic surfactant octyl sulfate (OS). This additive was chosen as it strongly adsorbs to positively charged surfaces of the AL and thereby induces a charge reversal. Figure 6a illustrates this behavior. At low OS concentrations, the electrokinetic potential of the AL particles is positive, reflecting their positive charge. Within increasing OS concentration, the potential decreases, and vanishes at a concentration around 0.4 mM. Upon further addition of OS, the potential decreases further, whereby the particles accumulate a negative charge. When NaCl is being added, the magnitude of the charge decreases somewhat, but the overall behavior remains the same.

Figure 6b shows the corresponding electrokinetic potentials for the SL particles. The particles remain negatively charged, and the addition of OS increases the magnitude of their charge, which suggests that OS adsorbs to these negatively charged particles too. Adding NaCl, the magnitude of the potential decreases.

Let us now focus on the aggregation behavior in the presence of OS. Given the high charge density of the SL particles, these suspensions remain stable for all conditions investigated. This aspect was verified by the appropriate light scattering measurements. On the other hand, the AL particles

aggregate rapidly near the charge reversal point, as illustrated in the left column of Fig. 7. When one plots the stability ratio versus the OS concentration, one observes a pronounced minimum near the charge reversal point. The aggregation near this minimum is fast, and slows down substantially when one moves away from it. Moreover, this minimum widens with the addition of NaCl. All these measurements are performed at much lower concentrations than the respective critical micelle concentration (CMC), which is 134 mM [37].

This behavior is easily understood since the particles are neutral near the charge reversal point, and thus they interact with attractive van der Waals forces only. These forces induce fast aggregation. Away from the charge reversal point, the particles become charged, and their aggregation is slowed down by repulsive double layer forces. Adding a monovalent electrolyte screens the double layer forces, thereby making them less repulsive, and thus reducing the stability ratio. A similar dependence of the stability ratio was observed for hematite particles in the presence of the same surfactant [38]. Analogous stability behavior was also reported in other systems undergoing a charge reversal, for example, for hematite particles versus pH [6], for amidine latex particles in the presence of tetraphenylborate or polystyrene sulfonate [33,39], or sulfate latex particles in the presence of aliphatic polyamines or polyethyleneimine [25,40-42].

Let us now focus on the heteroaggregation process in mixed suspensions containing AL and SL particles. Figure 8 illustrates the angular dependence of the apparent dynamic rates for different OS concentrations. Figure 8a shows the situation near the charge reversal point. One observes that heteroaggregation dominates the signal, as evident from the peak near 100°. As the OS concentration is being increased, homoaggregation becomes increasingly important. This fact can be inferred from Figs. 8b and 8c, as the maximum is reduced, and is replaced by a minimum near 120°. This minimum is characteristic for the presence of homoaggregates. Fig. 8d illustrates the extreme situation, where the signal is almost fully dominated by homoaggregation, but the contribution from heteroaggregation can be still detected, albeit barely. By fitting these apparent dynamic rates, the heteroaggregation rate coefficients can be extracted.

The respective heteroaggregation stability ratios are shown versus the OS concentration in Fig. 7a. At low OS concentrations, these ratios are below unity, since the heteroaggregation is enhanced by attractive double layer forces acting between the oppositely charged particles. When one adds NaCl to the system, the stability ratio becomes unity. The same situation was already encountered in the absence of OS, as illustrated in Fig. 4c. As the OS concentration is being increased, the heteroaggregation stability ratio starts to increase steeply. One observes that the error bars increase with increasing concentration, since the heteroaggregation process is increasingly masked by

homoaggregation. Nevertheless, the stability ratios for heteroaggregation can be reliably measured over almost three orders of magnitude.

The increase of the stability ratio for heteroaggregation can be explained by the onset of repulsive double layer forces between negatively charged surfaces. In this situation, however, one deals with an asymmetric situation where a strongly charged surface of the SL particles interacts with a weakly charged surface of the AL particle, which is decorated with adsorbed OS molecules. For this reason, the increase in the heteroaggregation stability ratios occurs at somewhat lower OS concentrations than for homoaggregation shown in Fig. 7a. This difference is more pronounced in the presence of added salt. For homoaggregation, one deals with a symmetric situation, where the two decorated AL particles interact. In this case, the double layer repulsion is weaker, and thus the onset is shifted to higher concentrations. A similar shift between the onset between slow heteroaggregation and slow homoaggregation was already observed in similar binary suspensions containing amidine and sulfate latex particles in the presence of cationic polyamines [25]. In the latter situation, however, the polyamines induced the charge reversal of the negatively charged sulfate particles.

The novel aspect of this study are reliable measurements of stability ratios for heteroaggregation above 100, see right column in Fig. 7. One observes that the dependence of these stability ratios on the OS concentration is similar as for homoaggregation. However, it appears that the slope of the stability plots for homoaggregation in the slow regime remains the same for different NaCl concentrations, while for heteroaggregation the slope is being modified. This observation is novel, since such high stability ratios for heteroaggregation were not reported in the literature so far. The only comparable data is the mentioned study by Cao et al. [25]. However, that study only reports heteroaggregation stability ratios up to 10, and based on these data considerations concerning the slope in the stability plots is hardly possible. This aspect further reflects the new feature of the present study, since heteroaggregation stability ratios can be reliably measured up values of several hundred.

Comparison with DLVO calculations. The present experimental studies were complemented with calculations of the stability ratios based on DLVO theory, which was extended to heteroaggregation [24,25]. The predictions contain no adjustable parameters. The Hamaker constant was taken to be 3.1×10^{-21} J, which is the same as used in earlier DLVO calculations involving the same particles [33]. This value is close to values extracted from direct force measurements involving similar, but larger latex particles [43,44]. While the Hamaker constant is expected to decrease with salt concentration [1], this effect is small, and becomes only appreciable high salt concentrations, where aggregation is fast anyway. The concentration of the monovalent salt was calculated from the solution composition. The diffuse layer potentials were approximated with the measured electrokinetic potentials, whereby empirical interpolating functions shown in Figs. 3 and 6 were used. In the PB calculations, three types

of boundary conditions were considered. Constant potential (CP, $p=0$), constant charge (CC, $p=1$), and constant regulation (CR) where $p=0.5$ was chosen. Both surfaces were assumed to regulate in the same way. While this assumption is not necessarily realistic, consideration of different regulation parameters for the two surfaces does not affect the calculated stability ratios substantially.

Consider first absolute rate coefficients in the fast regime, which is realized in concentrated monovalent salt solutions. The predicted values are given in Table 2. One observes that these values are about factor of two larger than the calculated ones. Similar discrepancies were observed earlier [24,25]. The most likely explanation is that the hydrodynamic resistance function is inaccurate at small distances due to roughness effects. While the Hamaker constant does also affect the calculated value, its influence is weak. Moreover, a similar discrepancy was also reported for larger particles, for which the Hamaker was known from direct force measurements [45].

Let us now discuss the stability ratios in the presence of NaCl, see Fig. 4. One observes that the DLVO calculation reflect the overall trends reasonably well. The agreement is very good for the SL-SL homoaggregation and for the AL-SL heteroaggregation. For the AL-AL homoaggregation, the trends in the stability ratios are predicted correctly, but the experimental values are substantially lower than the calculated ones. Similar discrepancies between experiment and DLVO calculations have been reported for positively charged particles earlier [6,24,25]. A possible reason of these discrepancies could be related from larger surface charge heterogeneity of these particles. The presence of such heterogeneities was shown to decrease the stability ratios substantially [6,46]. Another reason could be related to the high charge of the AL particles. For these particles, the DLVO theory predicts that the energy barrier is located at a separation distances well below of one nanometer. At these separations, DLVO theory is hardly expected to be accurate due to effects of surface roughness and the presence of additional solvation forces [43,47,48].

Effects of charge regulation are minor. While they can be clearly discerned in Fig. 4 in the case of homoaggregation processes, for heteroaggregation these charge regulation effects are so weak that the different curves cannot be distinguished on the scale of the graph. Similar observations concerning the applicability of DLVO theory for homoaggregation and heteroaggregation in monovalent salt solutions were made by some of us earlier [24,25].

Let us now focus on predictions of the stability ratios with DLVO theory in the presence of OS, see Fig. 7. In this case, these predictions capture the experimental data rather well. In particular, DLVO theory correctly predicts the increase in the stability ratio to occur at lower OS concentration for heteroaggregation than for homoaggregation. This difference is related to the fact that the double layer force is more repulsive in the asymmetric setting than in the symmetric one.

The main reason for the good agreement between experiment and DLVO theory is that the salt concentration remains low. They are typically below 10 mM, and never exceed 40 mM. Under these conditions, DLVO theory predicts that the energy barriers are located at distances of at least few nanometers. At these distances, DLVO theory is known to be quite accurate [47,48]. Nevertheless, one observes minor discrepancies in the slope of the stability curves, whereby the calculated ones are always steeper than the measured ones. These discrepancies are most important at the highest salt level of 30 mM, where the barrier separation distances are expected to be smallest. These slopes are further correctly predicted for the homoaggregation above the charge reversal point, where the AL particles are negatively charged, while more substantial deviations are present below the charge reversal point, where the particles are positively charged. This asymmetry reflects the same trend as observed in the presence of salt. The discrepancies in the slope can also be evidenced for heteroaggregation, especially at higher salt.

Charge regulation effects are most prominent for heteroaggregation, especially at low salt. One observes that CP conditions describe the experimental data quite well. On the other hand, the CC conditions predict an increase in the stability ratio for heteroaggregation at substantially lower concentration than experimentally observed. This observation suggests that the realistic boundary conditions are closer to CP, even though the data do not permit to estimate the regulation parameter in any reasonable precision. The reason for this strong influence of the charge regulation effects is that these effects substantially influence the strength of double layer forces for two dissimilarly charged surfaces, especially when one of these surfaces is weakly charged [49]. For two similarly charged surfaces, charge regulation these effects are much less important. For this reason, these effects are more modest for homoaggregation.

Conclusions

This study investigates heteroaggregation between amidine and sulfate latex particles in the presence of a short chain anionic surfactant by time-resolved multi-angle dynamic light scattering. This surfactant strongly adsorbs to amidine particles, which induces their charge reversal. The homoaggregation of these particles was equally studied, as they aggregate rapidly near the charge reversal point. The sulfate particles remain negatively charged and stable. The heteroaggregation process is probed in mixed suspensions of amidine and sulfate latex particles by multi-angle time-resolved dynamic light scattering, whereby one can clearly separate the contributions between homoaggregation and heteroaggregation. In this fashion, the heteroaggregation rate can be measured. The heteroaggregation rate is fast at low OS concentrations, where the two particles are oppositely charged. This rate slows down at higher OS concentrations due to double layer repulsion between the

negatively charged particles. However, the onset of this slow heteroaggregation occurs at lower OS concentrations than for homoaggregation. The reason for this shift is that the double layer repulsion between two OS-decorated amidine particles is weaker than between the sulfate particle and OS-decorated amidine particle. These measurements are compared with calculations based on DLVO theory. One finds that this theory is capable to predict the observed stability ratios quantitatively, especially at lower salt levels.

The novel contribution of this study is that we demonstrate that by appropriate choice of the two particles involved, the heteroaggregation aggregation rate coefficient can be measured over almost three orders of magnitude. This range is the widest ever reported in literature. This point represents the original aspect of the present work, since previous studies were able to access much smaller ranges only.

Acknowledgements

This work was supported by the Swiss National Science Foundation through awards 178759 and 159874 and the University of Geneva.

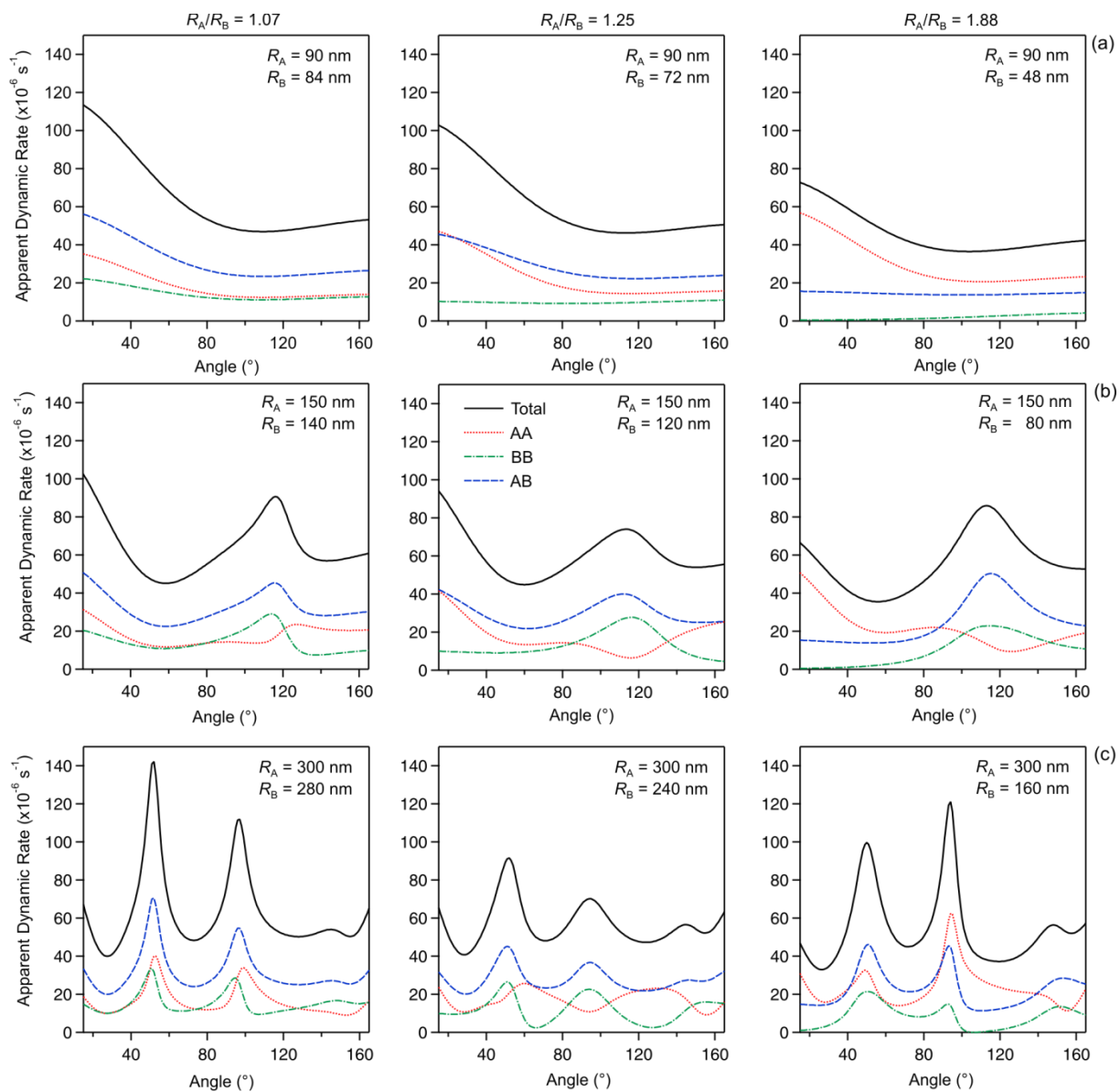
Table 1. Properties of the particles used.^{32,34}

Abbreviation		AL	SL
Mean particle radius (nm)	TEM ^a	151	125
	SLS ^b	149	117
	DLS ^c	153	123
Polydispersity (CV, %)	TEM ^a	5.7	3.1
	SLS ^b	6.5	7.2

^aTransmission electron microscopy (TEM) from the manufacturer. ^bAngle-resolved static light scattering (SLS). ^cDynamic light scattering (DLS) at a scattering angle of 90° [33].

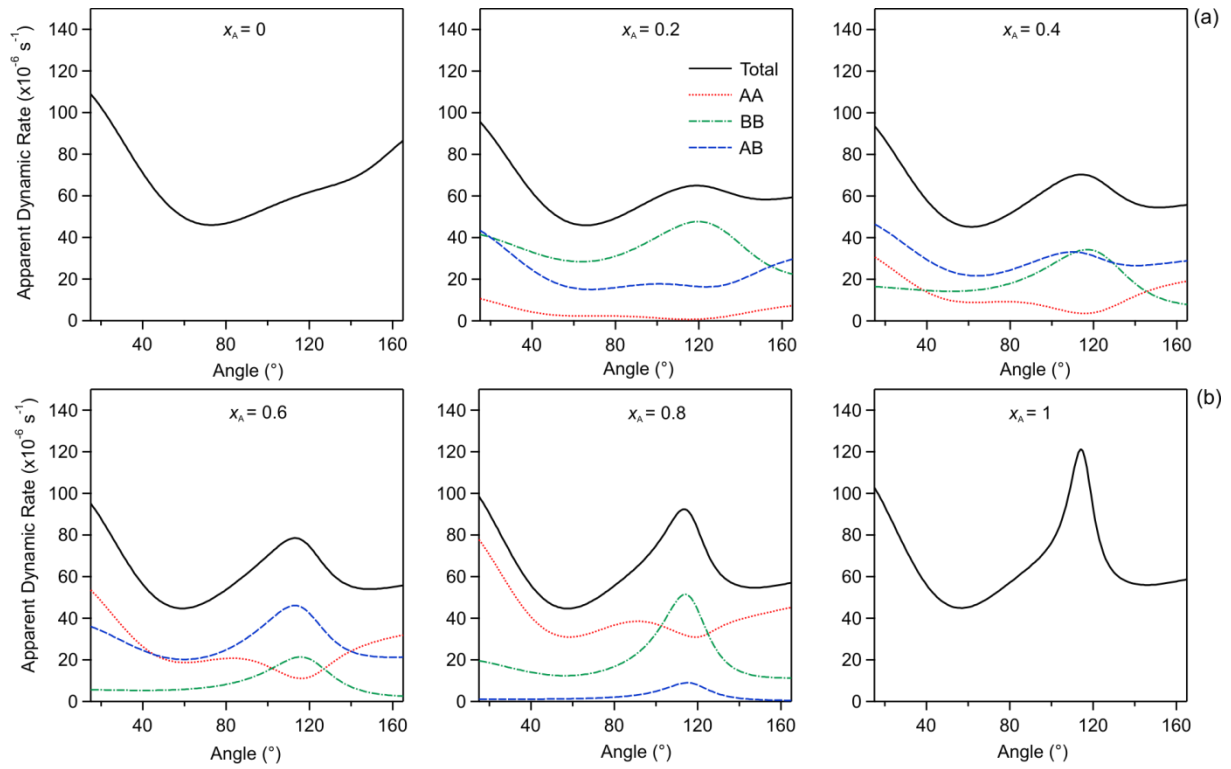
Table 2. Absolute fast aggregation rate coefficients in 0.8 M NaCl.

System	Rate coefficient ($\times 10^{-18} \text{ m}^3 / \text{s}$)	
	Experimental	DLVO Theory
AL-AL	3.1 \pm 0.2	6.79
SL-SL	2.8 \pm 0.2	6.79
AL-SL	3.1 \pm 0.2	6.89



This is a double-column figure. Please, do not print this text.

Figure 1. Variation of apparent dynamic rates versus the scattering angle for particle pairs of different sizes. The particle radii are indicated in each subfigure. The columns reflect the same ratios between the particle radii as indicated, while in the rows the radius of the larger particle is fixed. The calculations are carried out by fixing all aggregation rate coefficients at $3.0 \times 10^{-18} \text{ m}^3/\text{s}$ and the total particle number concentration at $7.0 \times 10^{13} \text{ m}^{-3}$. The number fractions of both particles are chosen to be the same ($x_A = x_B = 0.5$).



This is a double-column figure. Please, do not print this text.

Figure 2. Variation of apparent dynamic rates versus the scattering angle for particles A and B with radii of 150 nm and 120 nm. The number fraction of particles A is indicated in each subfigure, and increase from left to right, and from top to bottom. The calculations are carried out by fixing all aggregation rate coefficients at $3.0 \times 10^{-18} \text{ m}^3/\text{s}$ and the total particle number concentration at $7.0 \times 10^{13} \text{ m}^{-3}$.

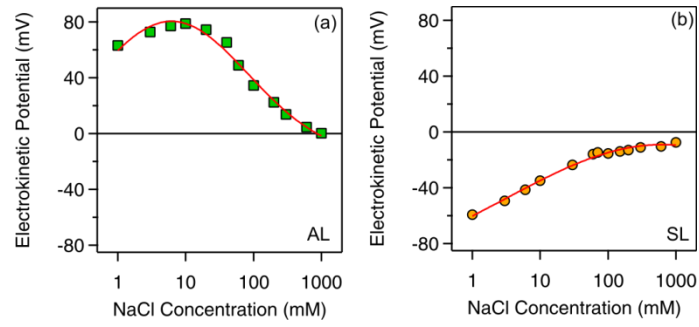
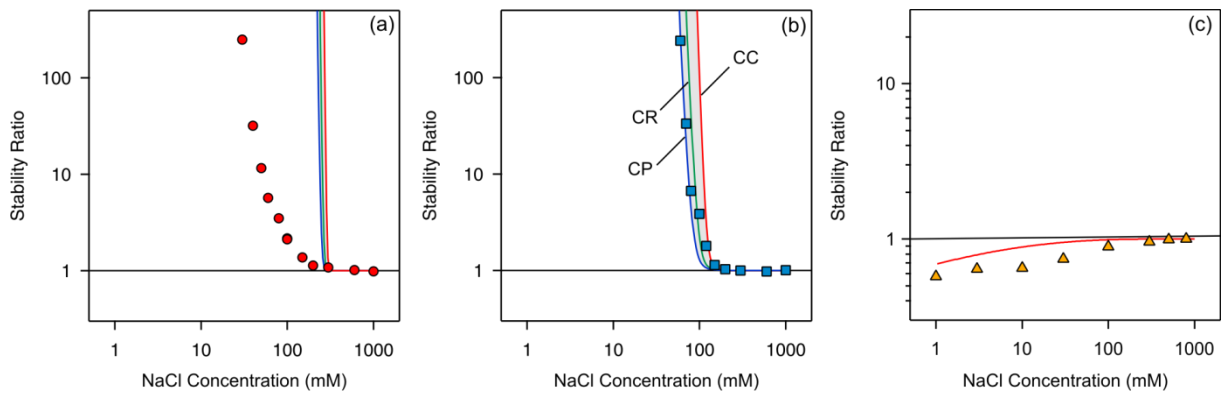


Figure 3. Electrokinetic potential (ζ -potential) obtained from electrophoretic mobility measurements versus the NaCl concentration for the latex particles investigated at pH 4.0. The solid lines are empirical interpolations that are used in the DLVO calculations. (a) AL and (b) SL.



This is a double-column figure. Please, do not print this text.

Figure 4. Stability ratios for the different aggregation processes versus the NaCl concentration at pH 4.0. The solid lines are predictions with DLVO theory with different boundary conditions, including constant potential (CP, $p = 0$), constant regulation (CR) with $p = 0.5$, and constant charge (CC, $p = 1$). Homoaggregation for (a) AL-AL and (b) SL-SL. (c) Heteroaggregation for AL-SL. On the scale of that graph, the different boundary conditions lead to identical results.

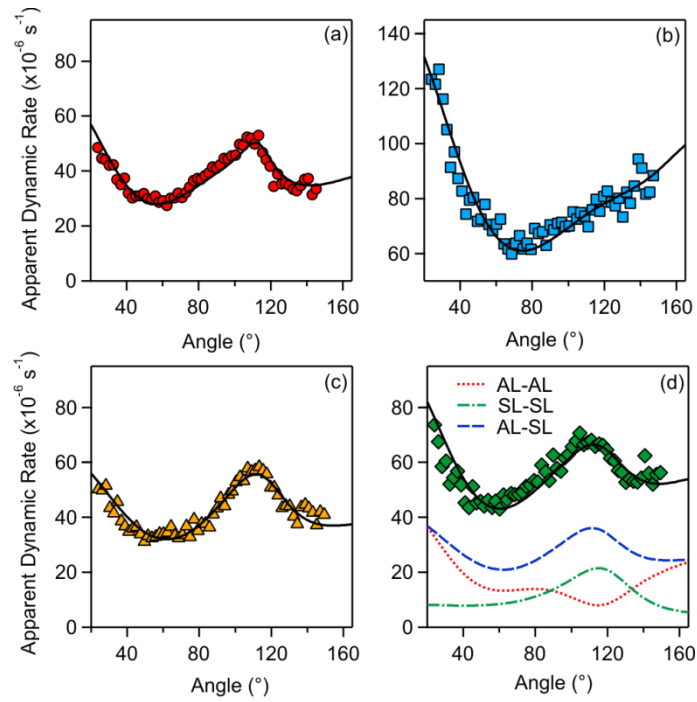


Figure 5. Apparent dynamic rates versus the scattering angle at pH 4.0. The points are the experimental results and the solid lines best fits with T-matrix theory. Homoaggregation in (a) AL and (b) SL suspensions with 0.8 M NaCl. (c) Pure heteroaggregation in 10 mM NaCl suspension. (d) Mixed homoaggregation and heteroaggregation in 0.8 M NaCl. Contributions from the different particle doublets are indicated with broken lines.

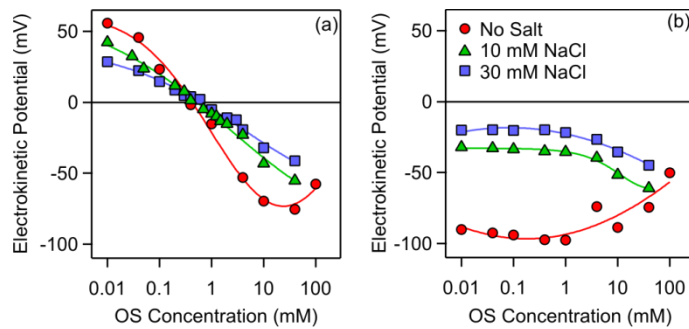


Figure 6. Electrokinetic potential (ζ -potential) obtained from electrophoretic mobility measurements versus the OS concentration at different levels of added NaCl and without added salt for the latex particles investigated at pH 4.0. (a) AL and (b) SL.

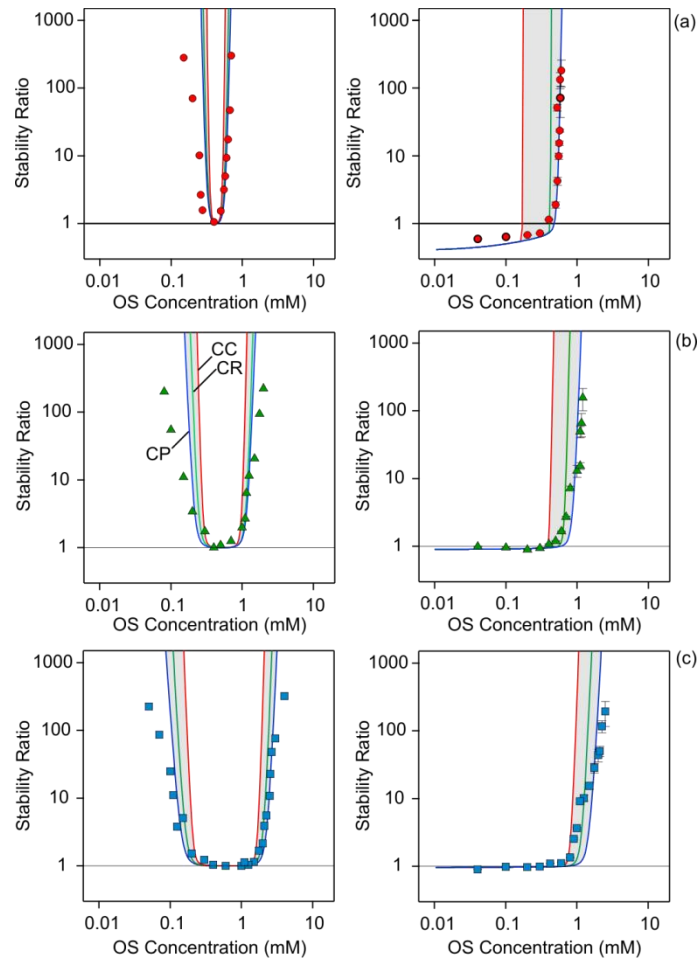


Figure 7. Stability ratios versus the OS concentration at different levels of added NaCl for the latex particles investigated at pH 4.0. The solid lines are predictions with DLVO theory with different boundary conditions, including constant potential (CP, $p = 0$), constant regulation (CR) with $p = 0.5$, and constant charge (CC, $p = 1$). Results for AL-AL homoaggregation is shown in the left column, while for AL-SL heteroaggregation in the right column. (a) No salt added and NaCl added at a concentration of (b) 10 mM and (c) 30 mM. Formation of SL-SL homoaggregates is negligible for all solution conditions shown.

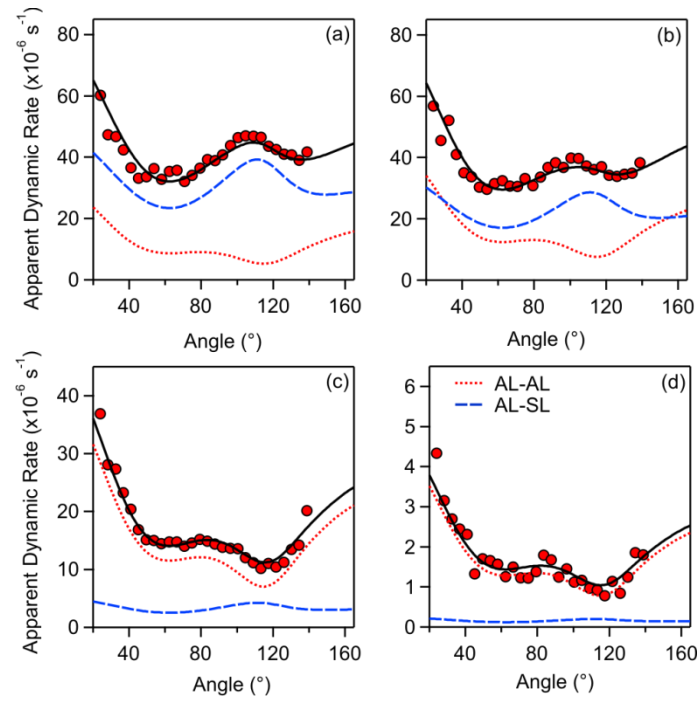


Figure 8. Apparent dynamic rates versus the scattering angle in solutions containing 30 mM NaCl and pH 4.0. The points are the experimental results and the solid lines best fits with T-matrix theory. OS concentration (a) 0.3 mM, (b) 0.8 mM, (c) 1.1 mM, and (d) 2.5 mM. Contributions from the different particle doublets are indicated with broken lines. The SL-SL homoaggregates do not form under any conditions shown.

References

- [1] W. B. Russel, D. A. Saville, W. R. Schowalter, *Colloidal Dispersions*, Cambridge University Press, Cambridge, 1989.
- [2] M. Elimelech, J. Gregory, X. Jia, R. A. Williams, *Particle Deposition and Aggregation: Measurement, Modeling, and Simulation*, Butterworth-Heinemann Ltd., Oxford, 1995.
- [3] K. L. Chen, S. E. Mylon, M. Elimelech, *Environ. Sci. Technol.* 40 (2006) 1516-1523.
- [4] T. Cao, I. Szilagyi, T. Oncsik, M. Borkovec, G. Trefalt, *Langmuir* 31 (2015) 6610–6614.
- [5] I. Szilagyi, A. Sadeghpour, M. Borkovec, *Langmuir* 28 (2012) 6211-6215.
- [6] M. Schudel, S. H. Behrens, H. Holthoff, R. Kretzschmar, M. Borkovec, *J. Colloid Interface Sci.* 196 (1997) 241-253.
- [7] T. Szabo, V. Toth, E. Horvath, L. Forro, I. Szilagyi, *Langmuir* 31 (2015) 42-49.
- [8] C. Schneider, M. Hanisch, B. Wedel, A. Jusufi, M. Ballauff, *J. Colloid Interface Sci.* 358 (2011) 62-67.
- [9] B. Balzer, M. K. M. Hruschka, L. J. Gauckler, *J. Colloid Interface Sci.* 216 (1999) 379-386.
- [10] D. Volodkin, V. Ball, P. Schaaf, J. C. Voegel, H. Möhwald, *Biochim. Biophys. Acta* 1768 (2007) 280-290.
- [11] S. Farrokhpay, *Adv. Colloid Interface Sci.* 151 (2009) 24-32.
- [12] J. Porubska, B. Alinec, T. G. M. van de Ven, *Colloid Surf. A* 210 (2002) 223-230.
- [13] R. Mezzenga, P. Schurtenberger, A. Burbidge, M. Michel, *Nature Mater.* 4 (2005) 729-740.
- [14] J. A. Redman, S. B. Grant, T. M. Olson, M. K. Estes, *Environ. Sci. Technol.* 35 (2001) 1798-1805.
- [15] B. Bolto, J. Gregory, *Water Res.* 41 (2007) 2301-2324.
- [16] V. Uricanu, J. R. Eastman, B. Vincent, *J. Colloid Interface Sci.* 233 (2001) 1-11.
- [17] A. M. Puertas, A. Fernandez-Barbero, F. J. de las Nieves, *Physica A* 304 (2002) 340-354.
- [18] R. O. James, A. Homola, T. W. Healy, *J. Chem. Soc. Farad. Trans. I* 73 (1977) 1436-1445.
- [19] H. Kihira, E. Matijevic, *Langmuir* 8 (1992) 2855-2862.
- [20] A. Y. Kim, J. C. Berg, *J. Colloid Interface Sci.* 229 (2000) 607-614.
- [21] A. M. Puertas, A. Fernandez-Barbero, F. J. de las Nieves, *J. Chem. Phys.* 114 (2001) 591-595.
- [22] A. M. Puertas, A. Fernandez-Barbero, F. J. de las Nieves, *J. Colloid Interface Sci.* 265 (2003) 36-43.
- [23] W. L. Yu, M. Borkovec, *J. Phys. Chem. B* 106 (2002) 13106-13110.
- [24] W. Lin, M. Kobayashi, M. Skarba, C. Mu, P. Galletto, M. Borkovec, *Langmuir* 22 (2006) 1038-1047.

- [25] T. Cao, T. Sugimoto, I. Szilagyi, G. Trefalt, M. Borkovec, *Phys. Chem. Chem. Phys.* 19 (2017) 15160 - 15171.
- [26] H. Lichtenfeld, V. Shilov, L. Knapschinsky, *Colloids Surf. A* 142 (1998) 155-163.
- [27] H. Holthoff, A. Schmitt, A. Fernandez-Barbero, M. Borkovec, M. A. Cabrerizo-Vilchez, P. Schurtenberger, R. Hidalgo-Alvarez, *J. Colloid Interface Sci.* 192 (1997) 463-470.
- [28] S. Barany, M. A. Cohen Stuart, G. J. Fleer, *Colloids Surf. A* 106 (1996) 213-221.
- [29] M. I. Mishchenko, D. W. Mackowski, *J. Quant. Spectrosc. Radiat. Transf.* 55 (1996) 683-694.
- [30] M. I. Mishchenko, L. D. Travis, A. A. Lacis, *Scattering, Absorption, and Emission of Light by Small Particles* University Press, Cambridge 2002.
- [31] W. L. Yu, E. Matijevic, M. Borkovec, *Langmuir* 18 (2002) 7853-7860.
- [32] D. J. Jeffrey, Y. Onishi, *J. Fluid Mech.* 139 (1984) 261-290.
- [33] T. Cao, G. Trefalt, M. Borkovec, *Langmuir* 34 (2018) 14368-14377.
- [34] R. W. O'Brien, L. R. White, *J. Chem. Soc. Farad. Trans. II* 74 (1978) 1607-1626.
- [35] G. Trefalt, I. Szilagyi, M. Borkovec, *J. Colloid Interf. Sci.* 406 (2013) 111-120.
- [36] R. Pericet-Camara, G. Papastavrou, S. H. Behrens, M. Borkovec, *J. Phys. Chem. B* 108 (2004) 19467-19475.
- [37] R. Ranganathan, L. Tran, B. L. Bales, *J. Phys. Chem. B* 104 (2000) 2260-2264.
- [38] M. Kobayashi, S. Yuki, Y. Adachi, *Colloid Surf. A* 510 (2016) 190-197.
- [39] G. Gillies, W. Lin, M. Borkovec, *J. Phys. Chem. B* 111 (2007) 8626-8633.
- [40] J. Gregory, *J. Colloid Interface Sci.* 42 (1973) 448-456.
- [41] I. Szilagyi, A. Polomska, D. Citherlet, A. Sadeghpour, M. Borkovec, *J. Colloid Interf. Sci.* 392 (2013) 34-41.
- [42] I. Szilagyi, D. Rosicka, J. Hierrezuelo, M. Borkovec, *J. Colloid Interf. Sci.* 360 (2011) 580-585.
- [43] M. Moazzami-Gudarzi, G. Trefalt, I. Szilagyi, P. Maroni, M. Borkovec, *J. Phys. Chem. C* 119 (2015) 15482-15490.
- [44] A. M. Smith, P. Maroni, M. Borkovec, *Phys. Chem. Chem. Phys.* 20 (2018) 158-164.
- [45] F. J. Montes Ruiz-Cabello, G. Trefalt, Z. Csendes, P. Sinha, T. Oncsik, I. Szilagyi, P. Maroni, M. Borkovec, *J. Phys. Chem. B* 117 (2013) 11853-11862.
- [46] H. Kihira, N. Ryde, E. Matijevic, *J. Chem. Soc. Faraday Trans.* 88 (1992) 2379-2386.
- [47] J. Israelachvili, *Intermolecular and Surface Forces*, Academic Press, London, 2011.
- [48] G. Trefalt, T. Palberg, M. Borkovec, *Current Opin. Colloid Interf. Sci.* 27 (2017) 9-17.
- [49] G. Trefalt, S. H. Behrens, M. Borkovec, *Langmuir* 32 (2016) 380-400.